European Polymer Journal 75 (2016) 200–209

Contents lists available at ScienceDirect

European Polymer Journal

journal homepage: www.elsevier.com/locate/europolj

Macromolecular Nanotechnology

Development of multifunctional polymer nanocomposites with carbon-based hybrid nanostructures synthesized from ferrocene

Juan Riquelme [a], Cristhian Garzón [a], Carlos Bergmann [b], Julian Geshev [c], Raúl Quijada [a,*]

[a] Departamento de Ingeniería Química y Biotecnología, Facultad de Ciencias Físicas y Matemáticas, Universidad de Chile, Santiago, Chile
[b] Laboratório de Materiais Cerâmicos, Departamento de Materiais, Universidade Federal do Rio Grande do Sul (UFRGS), Porto Alegre, Brazil
[c] Instituto de Física, Universidade Federal do Rio Grande do Sul (UFRGS), Porto Alegre, Brazil

ARTICLE INFO

Article history:
Received 15 October 2015
Received in revised form 1 December 2015
Accepted 11 December 2015
Available online 12 December 2015

Keywords:
Carbon-base fillers
Ferrocene
Nanocomposites
Magnetic polymers
Mechanical properties

ABSTRACT

This paper proposes the development of isotactic polypropylene (iPP) nanocomposites with magnetic carbon-based hybrid fillers, which contain magnetite, by melt mixing at 190 °C. The carbon-based fillers such as carbon nanotubes (CNTs) were synthesized via chemical vapor deposition (CVD), using ferrocene as catalyst and precursor synthesis, and using silica (SiO_2) or thermally reduced graphene oxide (TrGO) as support, obtaining $SiO_2/CNT_{Magnetite}$ and $TrGO/CNT_{Magnetite}$ hybrid nanostructures, respectively. Mechanical, electrical and magnetic behaviors of the iPP nanocomposites with magnetic CNTs were evaluated; their performance against iPP composites with commercial CNTs was compared. The results show that the electrical conductivity of the iPP nanocomposites is not affected by the presence of magnetite, reaching a percolation threshold similar to that obtained in iPP nanocomposites with commercial CNTs. Likewise, the presence of CNTs with magnetic particles changes the diamagnetic nature of the polymeric matrix, transforming it into a ferromagnetic composite at low filler concentrations (2 wt.%).

1. Introduction

In the recent decades, the development of polymer nanocomposites by incorporating particles of nanometric sizes to polymeric matrices has given rise to multifunctional materials with high mechanical, electrical, barrier, and thermal properties, among others, which can be used in various fields ranging from electronics to aerospace industry [1,2]. The final properties of the nanocomposites are strongly affected by the type (organic and inorganic natural or synthetic) of nanoparticles used as filler so the choice of these plays a key role in enhancing properties. Carbon nanotubes (CNTs) have been considered as unique reinforcing the development of different polymer composites due to their outstanding properties such as high electrical conductivity ($\sim 10^6$ S/m), high mechanical strength (−50 GPa) and low density, making them useful in a wide range of industrial applications [3,4].

Recently, polymeric nanocomposites with magnetic properties have attracted great interest both for the scientific value of understanding their properties and also for their numerous applications. Examples of highlighted magnetic polymer nanocomposites can be found in the areas of development of sensors and transducers, electronic devices, magnetic storage,

* Corresponding author.
E-mail address: raquijad@ing.uchile.cl (R. Quijada).

http://dx.doi.org/10.1016/j.eurpolymj.2015.12.007
0014-3057/

electromagnetic and microwave absorption, magnetic actuators, environmental remediation and treatment of diseases [5–8]. For these applications it has been reported a wide variety of polymer composites using as magnetic nanoparticles as filler such as iron-based compounds, cobalt and nickel particles [9–15].

Developments of polymeric composites with carbon-based fillers (either graphene or CNTs) decorated with magnetic particles, such as magnetite and other compounds, permit the use of the properties of these structures and impart magnetic properties to the matrix. A disadvantage of these methods is that a pre-functionalization of carbon-based structures is required to add the magnetic particles on the surface of these, becoming the more expensive and complex processes [8,16–18]. It is well know that ferrocene ($Fe(C_5H_5)_2$) is an organometallic compound consisting of two cyclopentadienyl rings bonded by an iron atom used to produce magnetic particles [19,20], magnetic polymer nanocomposites [21–23], and as an alternative to produce feasible CNTs-magnetic particles because of its ability to serve as both catalyst and precursor of the CNT synthesis as reported in previous studies [24–26].

The present work aims to develop magnetic isotactic polypropylene (iPP) nanocomposites with carbon-based hybrid nanostructures synthesized from ferrocene, through the technique of chemical vapor deposition (CVD) at low temperature (750 °C), and using nanoparticles (high surface area) of silica (SiO_2) or thermally reduced graphene oxide (TrGO) as support material. According to previous studies [24,25], the surface area of the support material plays a fundamental role in the nucleation and growth of CNTs, being the reason for our choice of TrGO. This method allows obtaining magnetic particles of magnetite (Fe_3O_4) incorporated in the structure of the CNTs. The aim is to observe how the presence of these magnetic particles affects mechanical and electrical properties of polymeric nanocomposites, comparing their performance against iPP nanocomposites with commercial carbon nanotubes (CNT_{Com}), which have no magnetic nanoparticles in its structure.

2. Experimental section

2.1. Materials

A commercial grade isotactic polypropylene from Petroquim S.A. (Chile) (PP2621) with a melt flow rate of 26 g/10 min (2.16 kg/230 °C) (Norm ASTM D-1238/95), M_w = 195 kg/mol, M_n = 71 kg/mol, PDI = 2.7 and melting point of 160 °C was used as matrix. Nanopowder silica (Aerosil 200) of high surface area (~200 m^2/g) provided by Evonik Industries [24,25], and thermally reduced graphene oxide (TrGO) with surface area of ~261 m^2/g synthesized according to Ref. [27], were used as support material. As catalyst and precursor in the synthesis of the CNTs, ferrocene (98 wt.% $Fe(C_5H_5)_2$) supplied by Sigma Aldrich was used. The commercial multiwalled carbon nanotubes (CNT_{Com}) were obtained from Bayer Material Science AG (Germany) (Baytubes C150P). Based on the datasheet information provided by Bayer, they are characterized by a purity higher than 95 wt.%, number of walls between 2 and 15, an outer mean diameter of 13–16 nm, an inner mean diameter of 4 nm, length between 1 and >10 μm. Irganox 1010 was used as antioxidant agent during the composite preparation.

2.2. Synthesis of carbon nanotubes (CNTs)

The $SiO_2/CNT_{Magnetite}$ or $TrGO/CNT_{Magnetite}$ hybrid nanostructures were synthesized in a CVD apparatus, composed basically of a 30 mm inner diameter quartz glass tube placed into a cylindrical furnace that can slide along the tube [24,25]. Highly pure helium gas was pumped into the tube reactor at 300 sccm ($5 * 10^{-6}$ m^3/s) when SiO_2 was used, and 200 sccm ($3.33 * 10^{-6}$ m^3/s) when TrGO was used. The SiO_2 (or TrGO) nanopowder was used as substrate for the nucleation and growth of CNTs. Ferrocene was used as iron and carbon precursor. The synthesis temperature was 750 °C with a ramp up ratio of 30 °C/min. The employed dwell time was 2 min.

For the synthesis of $SiO_2/CNT_{Magnetite}$ or $TrGO/CNT_{Magnetite}$ hybrid nanoparticles, 0.1 g of ferrocene is placed inside a smaller quartz tube that acts as a crucible. Half of this crucible is placed outside and half inside the furnace. The part of the crucible outside the furnace is where the ferrocene is placed, and ~0.002 or ~0.005 g of SiO_2 or TrGO, respectively, are placed at the half of the crucible inside the furnace. The temperature is set to increase until it reaches the temperature required. Subsequently, the oven is heated at 30 °C/min rate and once the required temperature is reached, the furnace slides over the ferrocene powder, which undergoes pyrolysis with nucleation and growth of CNTs occurring in a couple of minutes, similarly to that reported in previous studies [24,25].

2.3. Melt compounding

The composites were prepared using a Brabender Plasticorder (Brabender, Germany) internal mixer at 190 °C and a speed of 110 rpm. Approximately 30 g per mixing was produced, containing iPP, filler (CNT_{Com}, $SiO_2/CNT_{Magnetite}$ or $TrGO/CNT_{Magnetite}$), and a small spoonful (~0.005 g) of Irganox 1010 as antioxidant. Filler content ranges from 0 to 10 wt.% for CNT_{Com}, from 0 to 6 wt.% for $SiO_2/CNT_{Magnetite}$, and was constant in 2 wt.% for $TrGO/CNT_{Magnetite}$. First, iPP was mixed with antioxidant and subsequently half amount of the polymer (~13 g) was added to the mixer operated at 110 rpm. After 2 min the polymer is melted and the filler was added for 3 min. Finally, the rest of the polymer pellets were added and the speed of the mixer was held at 110 rpm for 10 min. Therefore, the total mixing time was around 15 min.

2.4. Characterization

X-ray diffraction (XRD) analysis was performed on a Siemens D-5000 diffractometer with scintillation detector diffraction system and Bragg–Brentano geometry operating with a Cu $K\alpha_1$ radiation source filtered with a graphite monochromator (λ = 1.5406 Å) at 40 kV and 30 mA in the 2θ range of 2–80° at the scan rate of 0.02°/s. The synthesized nanoparticles were evaluated regarding its structure with a Raman spectroscope, model Renishaw inVia Spectrometer System. The experiments were performed at room temperature, at a range of 0–3100 cm^{-1} using a laser of 514 nm. The morphology of nanoparticles was analyzed using a scanning electron microscope (SEM, FEI Inspect F50). The morphology and microstructure of the nanoparticles were determined by transmission electron microscopy (TEM) in a Tecnai ST F20 FEG-S/TEM operated at 200 kV, equipped with an Energy Dispersive X-ray analysis system (EDS).

Magnetic characterization of nanoparticles and nanocomposites was performed through a EZ9 MicroSense vibrating sample magnetometer (VSM) at room temperature with the magnetic field (H) ranging between −2.0 kOe and +2.0 kOe. Young's modulus and elongation at break of nanocomposites were tested on a HP model D-500 dynamometer according to ASTM D638-10 at ~25 °C. For these tests, samples bone type with length overall of 120 mm, distance between grips of 80 mm, width of narrow section of 11.5 mm and thickness of 1 mm were tested at a rate of 50 mm/min at room temperature. Results are the average values out of five measurements (typical deviation ca. 5%). For the electric resistivity, a megohmmeter (Megger BM11) with a highest voltage of 1200 V was used. With this set-up, the standard two-points method was used. For each electrical value displayed in this contribution, at least four samples were prepared and four measurements for each one were carried out. In general, differences around one order of magnitude were detected in the non- percolated samples having low conductivity values (~10^{-9} S/cm). For percolated samples, otherwise the experimental error for conductivities was less than 50%. For these tests, samples of 40 × 16 mm^2 and a thickness of 2 mm were used.

3. Results and discussions

3.1. Carbon-based hybrid nanoparticles

Different carbon-based hybrid nanoparticles such as $SiO_2/CNT_{Magnetite}$ and $TrGO/CNT_{Magnetite}$ were synthetized by CVD at low temperature, by using SiO_2 and TrGO as support, respectively.

3.1.1. Evaluation of the composition and morphology of CNTs

The X-ray diffraction (XRD) allows to determine the chemical composition of the synthesized nanoparticles. Fig. 1 (a) and (b) shows XRD patterns of the particles produced by using SiO_2 and TrGO, respectively as support for CNTs synthesis by thermal degradation of ferrocene. Diffraction patterns of the $SiO_2/CNT_{Magnetite}$ and $TrGO/CNT_{Magnetite}$ hybrid nanoparticles were very similar for both cases. Characteristic diffraction peaks of Fe_3O_4 related with (220), (311), (400), (511) and (440) planes, emerge from the hybrid particles, which correspond to the cubic phase of Fe_3O_4 with a face-centered cubic (fcc) structure of magnetite (JCPDS card No. 00-019-0629), with a lattice parameter of a = 8.396 Å [28–31]. Additionally, Fig. 1 (a) and (b) shows the characteristic diffraction peaks of Fe, (110) and (200), which correspond to the body-centered cubic (bcc) structure of Iron (JCPDS card No. 00-006-0696), and diffraction peaks associated with graphite, (002) which correspond to the hexagonal structure of Graphite-2H (JCPDS card No. 00-041-1487) was further observed confirming that under the reaction conditions the CNTs were formed [24,25,32], because the SiO_2 and TrGO used as support do not have characteristic peaks.

The formation of magnetite (Fe_3O_4) is due to the groups oxygenates (hydroxyl, epoxide, carboxyl and carbonyl functional groups) present in the TrGO [33], and the hydrophilic nature of the silica used as supports. The silica comes usually from synthesis through the sol/gel method, which uses an aqueous solvent for the production, causing the silica possesses silanol

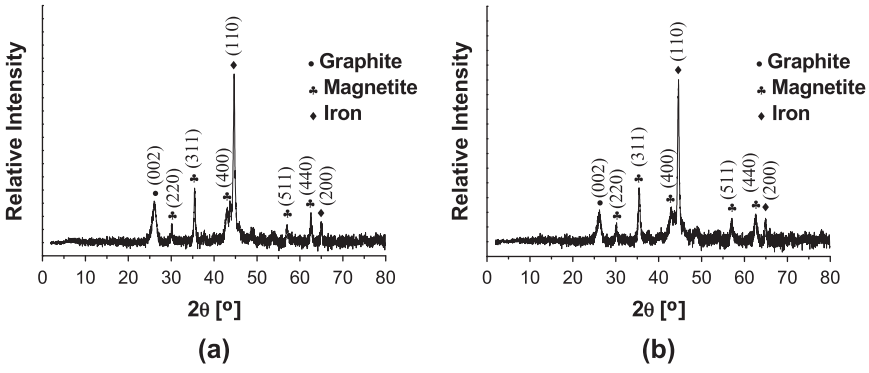

Fig. 1. XRD patterns of the (a) $SiO_2/CNT_{Magnetite}$ and (b) $TrGO/CNT_{Magnetite}$ hybrid nanoparticles.

(either free or neighborhood) or geminal groups in its structure. These groups make the silica has a hydrophilic nature, and therefore may have traces of humidity [34,35]. Thus, Fe^{2+} ions from the decomposition of ferrocene can attach to the groups oxygenates present in the SiO_2 and TrGO, through the thermal treatment to produce Fe_3O_4 on the surface of the substrate [9,36–39].

Fig. 2 shows the Raman spectra obtained for different CNTs synthesized from ferrocene using SiO_2 or TrGO as substrate. In both cases the presence of multiwall carbon nanotubes was evidenced, as in the high frequency spectrum the two characteristic bands of CNTs were obtained. One of these bands indicates the peak of the graphite (called band G) close to the $\sim$1600 cm^{-1}, and the other band (band D) is associated with defects and disorder of the structure, around $\sim$1380 cm^{-1}. Additionally a band called G′ at $\sim$2650 cm^{-1}, characteristic for carbon compounds of sp^2 hybridized was evidenced, ensuring the presence of CNTs. In the low-frequency spectrum (between 100 and 300 cm^{-1}), there is a second characteristic region for CNTs, called radial breathing mode (RBM) which is visible to those CNTs having diameters less than 2 nm. In our case, however, there were not evidenced peaks in this region of the spectrum, since the average diameter of the nanoparticles was higher than the limit set, so there is only MWCNT after synthesis [24,40].

The SEM and TEM images shown in Fig. 3 confirmed the presence of CNTs. The images obtained for CNTs on silica (Fig. 3 (a)) and TrGO (Fig. 3(b)) show that the nanotubes possess an average diameter of 20–40 nm, proportional to the size of the magnetite nanoparticles ($\sim$40 nm for SiO_2 and $\sim$20 nm for TrGO), which was confirmed by the TEM images for the SiO_2/$CNT_{Magnetite}$ and TrGO/$CNT_{Magnetite}$ hybrid nanoparticles in Fig. 3(c) and (d), respectively. According to the results shown by the Raman spectroscopy, and SEM and TEM images, the nucleation and growth of CNTs occurred on the substrate, forming entanglements of these. Noteworthy is the presence of magnetic nanoparticles inside CNTs, and decorating both the surface CNTs as surface TrGO sheets as indicated by the black arrows (Fig. 3(c) and (d)). A possible explanation for the mechanism of growth of CNTs on TrGO sheets is related to the widely-accepted "*tip-growth model*" [41]. Our observations confirm the findings of other authors (via ferrocene pyrolysis) [42–46], that the remaining metal catalyst nanoparticles are concentrated within and the top of CNTs, which is a clear illustration of the proposed growth mechanism.

3.1.2. Magnetic response of carbon-based hybrid nanoparticles

The magnetic properties of SiO_2/$CNT_{Magnetite}$ and TrGO/$CNT_{Magnetite}$ 3D hybrid nanoparticles are investigated through the magnetization (M) versus magnetic field (H) analysis using a vibrating sample magnetometer at room temperature. As seen in Fig. 4, the system presents hysteresis loops with coercivity of 550 ± 5 and 215 ± 5 Oe for SiO_2/$CNT_{Magnetite}$ and TrGO/$CNT_{Magnetite}$, respectively. These parameters and the shape of the loops indicate that the samples represent two magnetic behaviors. The SiO_2/$CNT_{Magnetite}$ nanoparticles (Fig. 4(a)) show a ferromagnetic behavior while the TrGO/$CNT_{Magnetite}$ nanoparticles (Fig. 4(b)) present a mixture of both ferromagnetic and superparamagnetic characteristics. The difference in the coercivity values presented by our SiO_2/$CNT_{Magnetite}$ and TrGO/$CNT_{Magnetite}$ hybrid nanoparticles is, most probably, due to the small size of the magnetic nanoparticles (see Fig. 3(a)) as also reported by other investigators [10,47], given that when TrGO is used as a substrate, there is a large surface area where iron can be deposited, resulting in a nucleation on greater number of small nanoparticles.

The values of the saturation magnetization (M_s) of pure Fe_3O_4 reported in the literature vary between 49 and 84.5 emu/g [9,28,32,48–50], while that estimated for our SiO_2/$CNT_{Magnetite}$ and TrGO/$CNT_{Magnetite}$ hybrid nanoparticles is 40 ± 1 emu/g, i.e., a value smaller than that of pure Fe_3O_4, possibly attributed to the nanoscale size of the Fe_3O_4 nanoparticles [9].

3.2. Polymeric nanocomposites with carbon-based hybrid nanoparticles

Different types of CNTs (CNT_{Com}, SiO_2/$CNT_{Magnetite}$ and TrGO/$CNT_{Magnetite}$) were used as filler to determine whether the characteristics of these affect the mechanical, electrical and magnetic behavior of nanocomposites prepared.

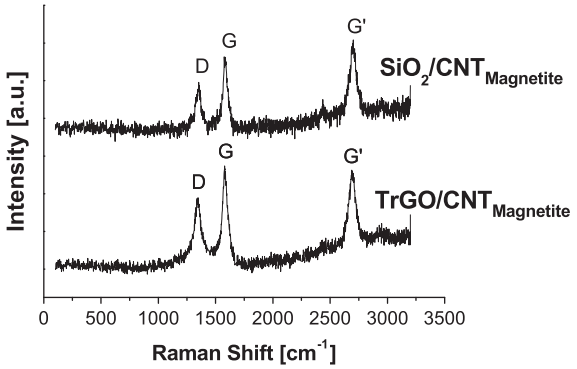

Fig. 2. Raman spectra obtained for SiO_2/$CNT_{Magnetite}$ and TrGO/$CNT_{Magnetite}$ hybrid nanoparticles.

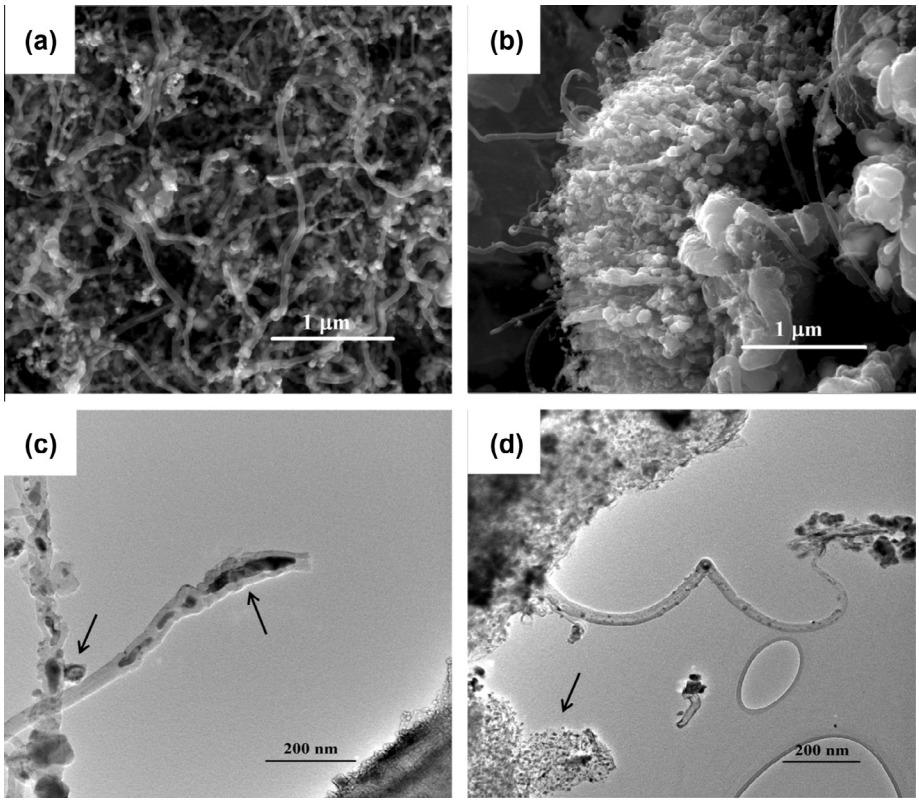

Fig. 3. SEM images of (a) $SiO_2/CNT_{Magnetite}$ and (b) $TrGO/CNT_{Magnetite}$, TEM images of (c) $SiO_2/CNT_{Magnetite}$ and (d) $TrGO/CNT_{Magnetite}$ hybrid nanoparticles.

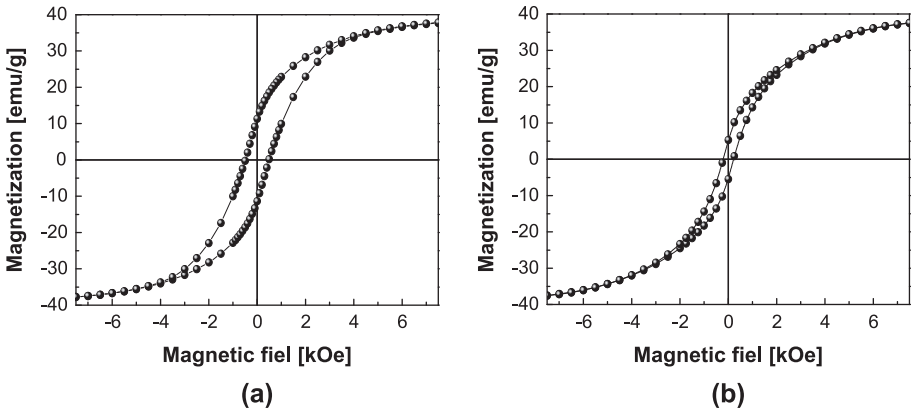

Fig. 4. Magnetization hysteresis cycles for (a) $SiO_2/CNT_{Magnetite}$ and (b) $TrGO/CNT_{Magnetite}$ hybrid nanoparticles.

3.2.1. Mechanical behavior of nanocomposites

The results of the effect of adding CNTs (CNT_{Com} and $SiO_2/CNT_{Magnetite}$) on the Young's modulus and strain at break are shown in Fig. 5. It was observed that increasing the filler concentration there was an increase in the elastic module up to 10% (~230 MPa) with CNT_{Com} and 7% (~170 MPa) with $SiO_2/CNT_{Magnetite}$ using 6 wt.% of filler (Fig. 5(a)), reflecting increased material stiffness, product of transfer load from the matrix to filler [51]. Similar tendency was reported by Sengupta et al. [52] and Steurer et al. [33] by using carbon-based fillers.

The results showed that by increasing the CNTs concentration there is a decrease in elongation at break (Fig. 5(b)) of up to ~80% and ~50% with 6 wt.% of CNT_{Com} and $SiO_2/CNT_{Magnetite}$, respectively. This phenomenon is due to nanoparticles strongly restrict movement of the polymer chains when they are under stress, preventing the chains may be long upon, thus reducing the elongation of the composite [51,53]. Discrepancies in properties described above can result from the dimensions of the

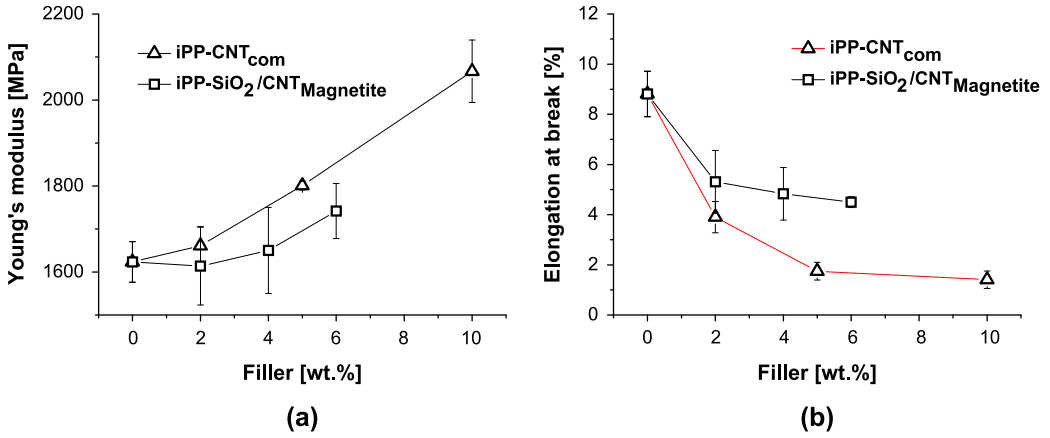

Fig. 5. Variation in (a) Young's modulus and (b) Elongation at break with the increase in the concentration of carbon-based filler.

CNTs used. The CNT_{Com} have an average diameter of ~13 nm and $SiO_2/CNT_{Magnetite}$ synthesized from ferrocene has a diameter of ~40 nm. The smaller diameter of CNT_{Com} contributes to stronger particle–matrix interface, and consequently, to a better charge transfer between the polymer and the filler thus achieving improved mechanical properties. Additionally, for a constant fraction of filler there exists as much CNT_{Com} that $SiO_2/CNT_{Magnetite}$ in the continuous phase, so the mobility of the polymer chains is smaller than in the case of the fillers synthesized from ferrocene, limiting the elongation of the final nanocomposite, such as presented in the study by Ayatollahi et al. [54]. The iPP composites with 2 wt.% of $TrGO/CNT_{Magnetite}$ showed a Young's modulus of ~1600 MPa and a decrease in the elongation at break of ~43%, values similar to those obtained with iPP composites with $SiO_2/CNT_{Magnetite}$ to the same filler concentration. Noteworthy is the highest Young's modulus achieved in the iPP nanocomposites with CNTs synthesized from ferrocene, compromising lesser degree elongation at break compared with iPP composites with CNT_{Com} at similar filler concentrations.

3.2.2. Electrical behavior of nanocomposites

Fig. 6 shows the variation in electrical conductivity of nanocomposites with the increase of the content of CNTs (of commercial origin and synthesized from ferrocene using SiO_2 as support), leading to the conclusion that the percolation threshold was independent of the type of filler used. The composites showed that, at concentrations above 2 wt.% of filler, the conductivity increased dramatically changing the conductive nature from insulating to semiconductor material. This increase in conductivity is due to the presence of continuous conduction pathways (percolated network) consisting of electrically conductive fillers (CNTs), by which the electrons travel along the polymer matrix [55]. Our results of conductivity for iPP composites with CNTs are very similar to those reported in other studies where the percolation threshold is below 5 wt.% of CNTs and the electrical conductivity is around 10^{-3} S/m [56–60].

As shown in Fig. 6, the electric conductivity curve of the iPP composites with CNT_{Com} overlaps with the curve obtained for the iPP composites with $SiO_2/CNT_{Magnetite}$. This was confirmed by analyzing the percolation threshold deducted according to classical percolation theory [55], where it was shown that the percolation threshold for iPP nanocomposites with CNT_{Com}

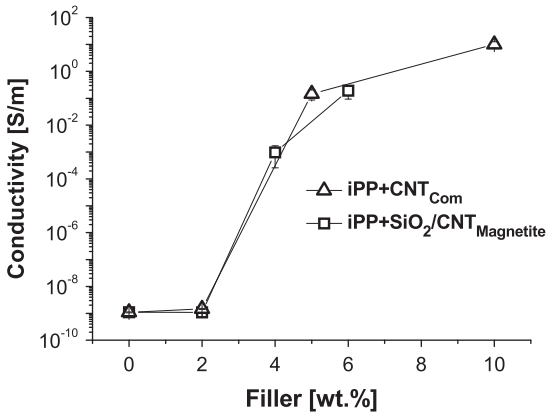

Fig. 6. Effect of carbon-based fillers on the electrical conductivity of isotactic polypropylene composites.

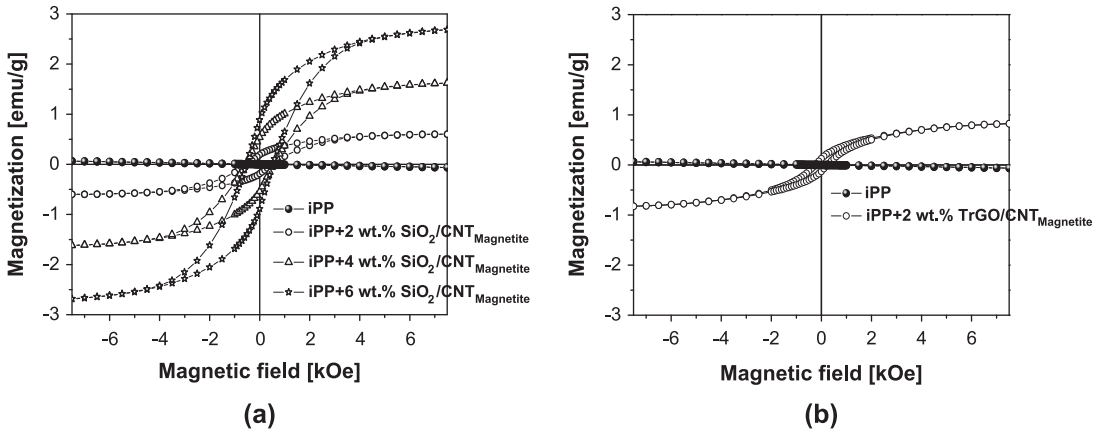

Fig. 7. Magnetic hysteresis cycles for iPP composites with (a) $SiO_2/CNT_{Magnetite}$ and (b) $TrGO/CNT_{Magnetite}$ hybrid nanoparticles.

Table 1
Magnetic parameters of the prepared nanocomposites.

Material	Coercitivity (Oe)	Saturation magnetization (M_s) (emu/g)	Remnant magnetization (M_r) (emu/g)
$SiO_2/CNT_{Magnetite}$	500	39	12
iPP + 2 wt.% of $SiO_2/CNT_{Magnetite}$	500	0.6	0.2
iPP + 4 wt.% of $SiO_2/CNT_{Magnetite}$	550	1.6	0.5
iPP + 6 wt.% of $SiO_2/CNT_{Magnetite}$	530	2.7	0.9
$TrGO/CNT_{Magnetite}$	215	39	5.5
iPP + 2 wt.% of $TrGO/CNT_{Magnetite}$	250	0.8	0.1

was very similar to that obtained for the case with $SiO_2/CNT_{Magnetite}$ as filler, reaching ~2.6 wt.% and ~2.8 wt.%, respectively. On the other hand, iPP composites with 2 wt.% of $TrGO/CNT_{Magnetite}$ had a conductivity in the range of $\sim10^{-9}$ S/m very similar to that achieved in the iPP nanocomposites with CNT_{Com} or $SiO_2/CNT_{Magnetite}$ to Similar concentrations, which was consistent with the values achieved in previous studies, both binary iPP composites and hybrids iPP composites with carbon-based nanofillers [27,56]. For this reason, the use of CNTs with magnetic particles ($SiO_2/CNT_{Magnetite}$ and $TrGO/CNT_{Magnetite}$) does not affect the performance of the electrical conductivity of the final nanocomposite, reaching conductivity values very close to those obtained using CNT_{Com} with a similar concentration.

3.2.3. Magnetic response of nanocomposites

The curves of the magnetic response of the polymer matrix and their nanocomposites with $SiO_2/CNT_{Magnetite}$ and $TrGO/CNT_{Magnetite}$ when subjected to an inductive field are shown in Fig. 7. It can be seen when the iPP matrix was subjected to a positive magnetic field, there is a negative magnetization response, causing the material was repelled by the inductor field. This behavior is typically presented by diamagnetic materials where the magnetic susceptibility: due to the absence of unpaired electrons in their outer structure, there is no net magnetic moments, thereby inducing a magnetic dipole in the opposite field direction [47].

On the other hand, Fig. 7(a) and (b) shows that iPP nanocomposites with different CNTs (synthetized from ferrocene) presented a different behavior from the neat iPP matrix. The diamagnetic nature of the iPP matrix at low concentrations (2 wt.%) of $SiO_2/CNT_{Magnetite}$ and $TrGO/CNT_{Magnetite}$ hybrid nanoparticles is modified, which become ferromagnetic ones. These nanocomposites, when subjected to a magnetic field, show a hysteresis response, i.e., they have variable susceptibility, also greater than zero. As noted above, this behavior is due to the presence of iron-based compounds with unpaired electrons in the *d* orbitals of the structure that engage with unpaired electrons from similar orbitals of neighboring atoms, thereby causing a magnetic dipole in the same direction of the induction field [47].

From the hysteresis curves plotted in Fig. 7 it is possible to obtain the most representative magnetic parameters of a ferromagnetic material, these are summarized in Table 1.

Was noted that the M_s and remnant magnetization (M_r) are parameters that depend on the amount of magnetic material in the nanocomposite, since increasing the filler content from 2 to 6 wt.% of $SiO_2/CNT_{Magnetite}$ there was an increase of more than twice the values of M_s and M_r with a tendency to approach the values obtained by the synthesized nanoparticles. This behavior has been reported by several authors [17,18,61], the explanation being that, with increasing concentration of filler, there will be a greater number of atoms with unpaired electrons in the *d* orbitals, facilitating coupling of electrons and generating a larger amount of magnetic dipoles in field direction, thereby increasing the saturation magnetization and remnant magnetization of the composite. Moreover, in Table 1 it can be seen that the values of coercivity for iPP nanocomposites with

$SiO_2/CNT_{Magnetite}$ were between ~500 and ~550 Oe, remaining practically constant from one compound to another. This can be attributed to the fact that the coercivity depends on the size of the magnetic particle that is magnetizing [47,62], and not on the concentration of magnetic phase; having in each case the same size distribution, greater differences in this property were not observed.

On the other hand, nanocomposites with $TrGO/CNT_{Magnetite}$ show a coercivity of ~250 Oe, close to the value reached by the synthesized nanoparticles (~215 Oe), and a value of M_s (~0.8 emu/g) similar to that achieved by iPP nanocomposites with a concentration of 2 wt.% of CNTs synthesized using SiO_2 as support.

4. Conclusions

This paper presented a route to develop magnetic polymeric nanocomposites by melt mixing of isotactic polypropylene (iPP) with CNTs synthesized from ferrocene (used as catalyst and precursor synthesis) and SiO_2 or TrGO as support materials, avoiding previously functionalized nanoparticles to the magnetic particles is incorporated. The CNTs multiwall were obtained with doped magnetite and metallic iron, which showed a saturation magnetization of ~39 emu/g and a coercivity which varied between ~215 and ~500 Oe according the substrate used. The incorporation of $SiO_2/CNT_{Magnetite}$ (or $TrGO/CNT_{Magnetite}$) hybrid nanoparticles to iPP matrix modified the diamagnetic nature of neat polymer, becoming the nanocomposite a ferromagnetic material with only 2 wt.% of filler. The electrical behavior of the iPP nanocomposite with $SiO_2/CNT_{Magnetite}$ (or $TrGO/CNT_{Magnetite}$) were similar to the performance presented by iPP nanocomposites with CNT_{Com}, so the incorporation of magnetic nanoparticles in carbon-based filler does not affect the performance of this property. However, the mechanical behavior of the iPP composites depends on the type of carbon-based filler used, since a high Young's modulus in the iPP nanocomposites with CNTs synthesized from ferrocene was achieved, compromising lesser degree elongation at break compared with iPP composites with CNT_{Com} at similar filler concentrations.

Acknowledgements

The authors would like to thank postdoctoral project FONDECYT N° 3150349, project FONDECYT N° 1130446 and CNPq–Brazil for financial support (Special Visiting Research Fellowship to Professor Raúl Quijada). Professor Raúl Quijada acknowledge the Millennium Nucleus of Chemical Processes and Catalysis (CPC), Grant number NC120082. It is also expressed the thanks to E.E. Mario Vergara, Chief of the Electrical Testing Unit (IDIEM)–Chile.

References

[1] Y. Jia, K. Peng, X. Gong, Z. Zhang, Creep and recovery of polypropylene/carbon nanotube composites, Int. J. Plast. 27 (2011) 1239–1251, http://dx.doi.org/10.1016/j.ijplas.2011.02.004.
[2] K. Chrissafis, D. Bikiaris, Can nanoparticles really enhance thermal stability of polymers? Part I: An overview on thermal decomposition of addition polymers, Thermochim. Acta 523 (2011) 1–24, http://dx.doi.org/10.1016/j.tca.2011.06.010.
[3] T. Filleter, A.M. Beese, M.R. Roenbeck, X. Wei, H.D. Espinosa, Tailoring the mechanical properties of carbon nanotube fibers, Nanotub. Superfib. Mater. (2014) 61–85, http://dx.doi.org/10.1016/B978-1-4557-7863-8.00003-7.
[4] H. Zhu, J. Njuguna, Nanolayered silicates/clay minerals: uses and effects on health, Heal. Environ. Saf. Nanomater. (2014) 133–146, http://dx.doi.org/10.1533/9780857096678.3.133.
[5] M. Castrillón García, Síntesis de nanopartículas magnéticas y su aplicación en nanocompuestos de matriz polimérica con propiedades magnéticas, Universidad de Zaragoza, 2012.
[6] R. Asmatulu, M.a. Zalich, R.O. Claus, J.S. Riffle, Synthesis, characterization and targeting of biodegradable magnetic nanocomposite particles by external magnetic fields, J. Magn. Magn. Mater. 292 (2005) 108–119, http://dx.doi.org/10.1016/j.jmmm.2004.10.103.
[7] T. Neuberger, B. Schöpf, H. Hofmann, M. Hofmann, B. Von Rechenberg, Superparamagnetic nanoparticles for biomedical applications: possibilities and limitations of a new drug delivery system, J. Magn. Magn. Mater. 293 (2005) 483–496, http://dx.doi.org/10.1016/j.jmmm.2005.01.064.
[8] J. Zhu, S. Wei, M. Chen, H. Gu, S.B. Rapole, S. Pallavkar, et al, Magnetic nanocomposites for environmental remediation, Adv. Powder Technol. 24 (2013) 459–467, http://dx.doi.org/10.1016/j.apt.2012.10.012.
[9] S. Zhu, J. Guo, J. Dong, Z. Cui, T. Lu, C. Zhu, et al, Sonochemical fabrication of Fe_3O_4 nanoparticles on reduced graphene oxide for biosensors, Ultrason. Sonochem. 20 (2013) 872–880, http://dx.doi.org/10.1016/j.ultsonch.2012.12.001.
[10] N.A.D. Burke, H.D.H. Stover, F.P. Dawson, Magnetic nanocomposites: preparation and characterization of polymer coated iron nanoparticles, Chem. Mater. 14 (2002) 4752–4761, http://dx.doi.org/10.1021/cm020126q.
[11] H. Nathani, R.D.K. Misra, Surface effects on the magnetic behavior of nanocrystalline nickel ferrites and nickel ferrite–polymer nanocomposites, Mater. Sci. Eng. B 113 (2004) 228–235, http://dx.doi.org/10.1016/j.mseb.2004.08.010.
[12] a.a. Novakova, V.Y. Lanchinskaya, a.V. Volkov, T.S. Gendler, T.Y. Kiseleva, M.a. Moskvina, et al, Magnetic properties of polymer nanocomposites containing iron oxide nanoparticles, J. Magn. Magn. Mater. 258-259 (2003) 354–357, http://dx.doi.org/10.1016/S0304-8853(02)01062-4.
[13] S. Goodwin, C. Peterson, C. Hoh, C. Bittner, Targeting and retention of magnetic targeted carriers (MTCs) enhancing intra-arterial chemotherapy, J. Magn. Magn. Mater. 194 (1999) 132–139, http://dx.doi.org/10.1016/S0304-8853(98)00584-8.
[14] S. Rudge, T. Kurtz, C. Vessely, L. Catterall, D. Williamson, Preparation, characterization, and performance of magnetic iron–carbon composite microparticles for chemotherapy, Biomaterials 21 (2000) 1411–1420, http://dx.doi.org/10.1016/S0142-9612(00)00006-5.
[15] S. Sershen, J. West, Implantable, polymeric systems for modulated drug delivery, Adv. Drug Deliv. Rev. 54 (2002) 1225–1235, http://dx.doi.org/10.1016/S0169-409X(02)00090-X.
[16] Z. Mitróová, N. Tomašovi, Č. Ová, G. Lancz, J.K. Č, I. Vávra, et al, Preparation and characterization of carbon nanotubes functionalized by magnetite nanoparticles, Olomouc (Czech Republic) (2010) 10–15.
[17] Y. Long, Z. Chen, J.L. Duvail, Z. Zhang, M. Wan, Electrical and magnetic properties of polyaniline/Fe_3O_4 nanostructures, Phys. B Condens. Matter. 370 (2005) 121–130, http://dx.doi.org/10.1016/j.physb.2005.09.009.
[18] J. Zhao, Y. Xie, M. Li, F. Xu, Z. Le, Y. Qin, et al, Preparation of magnetic-conductive $Mn_{0.6}Zn_{0.4}Fe_2O_4$–CNTs/PANI nanocomposites through hydrothermal synthesis coupled with in situ polymerization, Compos. Sci. Technol. 99 (2014) 147–153, http://dx.doi.org/10.1016/j.compscitech.2014.05.023.

[19] G.M. Bhalerao, A.K. Sinha, H. Srivastava, A.K. Srivastava, Synthesis and studies of growth kinetics of monodispersed iron oxide nanoparticles using ferrocene as novel precursor, Appl. Phys. A 95 (2009) 373–380, http://dx.doi.org/10.1007/s00339-008-5068-z.
[20] a. Bhattacharjee, A. Rooj, M. Roy, J. Kusz, P. Gütlich, Solventless synthesis of hematite nanoparticles using ferrocene, J. Mater. Sci. 48 (2013) 2961–2968, http://dx.doi.org/10.1007/s10853-012-7067-x.
[21] S.B. Clendenning, S. Han, N. Coombs, C. Paquet, M.S. Rayat, D. Grozea, et al, Magnetic ceramic films from a metallopolymer resist using reactive ion etching in a secondary magnetic field, Adv. Mater. 16 (2004) 291–296, http://dx.doi.org/10.1002/adma.200306262.
[22] M. Häußler, Q. Sun, K. Xu, J.W.Y. Lam, H. Dong, B.Z. Tang, Hyperbranched poly(ferrocenylene)s containing groups 14 and 15 elements: syntheses, optical and thermal properties, and pyrolytic transformations into nanostructured magnetoceramics, J. Inorg. Organomet. Polym. Mater. 15 (2005) 67–81, http://dx.doi.org/10.1007/s10904-004-2379-1.
[23] D. Scheid, G. Cherkashinin, E. Ionescu, M. Gallei, Single-source magnetic nanorattles by using convenient emulsion polymerization protocols, Langmuir 30 (2014) 1204–1209, http://dx.doi.org/10.1021/la404285c.
[24] A.G. Osorio, C.P. Bergmann, Effect of surface area of substrates aiming the optimization of carbon nanotube production from ferrocene, Appl. Surf. Sci. 264 (2013) 794–800, http://dx.doi.org/10.1016/j.apsusc.2012.10.134.
[25] A.G. Osorio, L.G. Pereira, J.B.M. da Cunha, C.P. Bergmann, Controlling the magnetic response of carbon nanotubes filled with iron-containing material, Mater. Res. Bull. 48 (2013) 4168–4173, http://dx.doi.org/10.1016/j.materresbull.2013.06.045.
[26] S. Vadahanambi, S.-H. Lee, W.-J. Kim, I.-K. Oh, Arsenic removal from contaminated water using three-dimensional graphene–carbon nanotube–iron oxide nanostructures, Environ. Sci. Technol. 47 (2013) 10510–10517, http://dx.doi.org/10.1021/es401389g.
[27] C. Garzón, H. Palza, Electrical behavior of polypropylene composites melt mixed with carbon-based particles: effect of the kind of particle and annealing process, Compos. Sci. Technol. 99 (2014) 117–123, http://dx.doi.org/10.1016/j.compscitech.2014.05.018.
[28] Y. Chen, Y. Wang, H. Zhang, X. Li, C. Gui, Z. Yu, Enhanced electromagnetic interference shielding efficiency of polystyrene/graphene composites with magnetic Fe_3O_4 nanoparticles, Carbon 82 (2014) 67–76, http://dx.doi.org/10.1016/j.carbon.2014.10.031.
[29] M. Liu, C. Chen, J. Hu, X. Wu, X. Wang, Synthesis of magnetite/graphene oxide composite and application for cobalt(II) removal, J. Phys. Chem. C 115 (2011) 25234–25240, http://dx.doi.org/10.1021/jp208575m.
[30] D. Sun, Q. Zou, G. Qian, C. Sun, W. Jiang, F. Li, Controlled synthesis of porous Fe_3O_4-decorated graphene with extraordinary electromagnetic wave absorption properties, Acta Mater. 61 (2013) 5829–5834, http://dx.doi.org/10.1016/j.actamat.2013.06.030.
[31] J. Zheng, H. Lv, X. Lin, G. Ji, X. Li, Y. Du, Enhanced microwave electromagnetic properties of Fe_3O_4/graphene nanosheet composites, J. Alloys Compd. 589 (2014) 174–181, http://dx.doi.org/10.1016/j.jallcom.2013.11.114.
[32] W. Jiao, M. Shioya, R. Wang, F. Yang, L. Hao, Y. Niu, et al, Improving the gas barrier properties of Fe_3O_4/graphite nanoplatelet reinforced nanocomposites by a low magnetic field induced alignment, Compos. Sci. Technol. 99 (2014) 124–130, http://dx.doi.org/10.1016/j.compscitech.2014.05.022.
[33] P. Steurer, R. Wissert, R. Thomann, R. Mülhaupt, Functionalized graphenes and thermoplastic nanocomposites based upon expanded graphite oxide, Macromol. Rapid Commun. 30 (2009) 316–327, http://dx.doi.org/10.1002/marc.200800754.
[34] R. Ojeda-López, I.J. Pérez-Hermosillo, J.M. Esparza-Schulz, A. Domínguez-Ortiz, Efecto de la temperatura de calcinación sobre la concentración de grupos silanoles en superficies de SiO_2 (SBA–15), Avances en Química 9 (2014) 21–28. <http://www.scopus.com/inward/record.url?eid=2-s2.0-84902147776&partnerID=tZOtx3y1>.
[35] X. Liang, Dispersibility, shape and magnetic properties of nano-Fe_3O_4 particles, Mater. Sci. Appl. 02 (2011) 1644–1653, http://dx.doi.org/10.4236/msa.2011.211219.
[36] T. Wang, Z. Liu, M. Lu, B. Wen, Q. Ouyang, Y. Chen, et al, Graphene–Fe_3O_4 nanohybrids: synthesis and excellent electromagnetic absorption properties, J. Appl. Phys. 113 (2013), http://dx.doi.org/10.1063/1.4774243.
[37] L. Xu, W. Zhang, Y. Ding, Y. Peng, S. Zhang, W. Yu, et al, Formation, characterization, and magnetic properties of Fe_3O_4 nanowires encapsulated in carbon microtubes, J. Phys. Chem. B 108 (2004) 10859–10862, http://dx.doi.org/10.1021/jp049318u.
[38] F. Cao, C. Chen, Q. Wang, Q. Chen, Synthesis of carbon–Fe_3O_4 coaxial nanofibres by pyrolysis of ferrocene in supercritical carbon dioxide, Carbon 45 (2007) 727–731, http://dx.doi.org/10.1016/j.carbon.2006.11.030.
[39] J. Zhang, J. Wang, H. Wang, L. Jia, Z. Qu, Y. Qian, Synthesis and magnetic properties of Fe_3O_4/helical carbon nanofiber nanocomposites from the catalytic pyrolysis of ferrocene, Chin. Sci. Bull. 56 (2011) 3199–3203, http://dx.doi.org/10.1007/s11434-011-4653-2.
[40] C. Domingo, G. Santoro, Espectroscopía Raman de nanotubos de carbono, Opt. Pura Y Apl. 40 (2007) 175–186.
[41] M. Kumar, Y. Ando, Chemical vapor deposition of carbon nanotubes: a review on growth mechanism and mass production, J. Nanosci. Nanotechnol. 10 (2010) 3739–3758, http://dx.doi.org/10.1166/jnn.2010.2939.
[42] H. Hou, A.K. Schaper, F. Weller, A. Greiner, Carbon nanotubes and spheres produced by modified ferrocene pyrolysis, Chem. Mater. (2002) 3990–3994, http://dx.doi.org/10.1021/cm021206x.
[43] X. Zhang, a. Cao, B. Wei, Y. Li, J. Wei, C. Xu, et al, Rapid growth of well-aligned carbon nanotube arrays, Chem. Phys. Lett. 362 (2002) 285–290, http://dx.doi.org/10.1016/S0009-2614(02)01025-4.
[44] D.M. Guldi, M. Marcaccio, D. Paolucci, F. Paolucci, N. Tagmatarchis, D. Tasis, et al, Single-wall carbon nanotube-ferrocene nanohybrids: observing intramolecular electron transfer in functionalized SWNTs, Angew. Chem. – Int. Ed. 42 (2003) 4206–4209, http://dx.doi.org/10.1002/anie.200351289.
[45] Y.T. Lee, N.S. Kim, J. Park, J.B. Han, Y.S. Choi, H. Ryu, et al, Temperature-dependent growth of carbon nanotubes by pyrolysis of ferrocene and acetylene in the range between 700 and 1000 °C, Chem. Phys. Lett. 372 (2003) 853–859, http://dx.doi.org/10.1016/S0009-2614(03)00529-3.
[46] A. Moisala, A.G. Nasibulin, D.P. Brown, H. Jiang, L. Khriachtchev, E.I. Kauppinen, Single-walled carbon nanotube synthesis using ferrocene and iron pentacarbonyl in a laminar flow reactor, Chem. Eng. Sci. 61 (2006) 4393–4402, http://dx.doi.org/10.1016/j.ces.2006.02.020.
[47] J.L. Wilson, Synthesis and magnetic properties of polymer nanocomposites with embedded iron nanoparticles, J. Appl. Phys. 95 (2004) 1439–1443, http://dx.doi.org/10.1063/1.1637705.
[48] M.A. Farghali, T.A.S. El-din, A.M. Al-enizi, R.M. El Bahnasawy, Graphene/magnetite nanocomposite for potential environmental application, Int. J. Electrochem. Sci. 10 (2015) 529–537.
[49] L. Ren, S. Huang, W. Fan, T. Liu, One-step preparation of hierarchical superparamagnetic iron oxide/graphene composites via hydrothermal method, Appl. Surf. Sci. 258 (2011) 1132–1138, http://dx.doi.org/10.1016/j.apsusc.2011.09.049.
[50] M. Zong, Y. Huang, Y. Zhao, L. Wang, P. Liu, Y. Wang, et al, One-pot simplified co-precipitation synthesis of reduced graphene oxide/Fe_3O_4 composite and its microwave electromagnetic properties, Mater. Lett. 106 (2013) 22–25, http://dx.doi.org/10.1016/j.matlet.2013.04.097.
[51] H. Zou, S. Wu, J. Shen, Polymer/silica nanocomposites: preparation, characterization, properties, and applications, Chem. Rev. 108 (2008) 3893–3957, http://dx.doi.org/10.1021/cr068035q.
[52] R. Sengupta, M. Bhattacharya, S. Bandyopadhyay, A.K. Bhowmick, A review on the mechanical and electrical properties of graphite and modified graphite reinforced polymer composites, Prog. Polym. Sci. 36 (2011) 638–670, http://dx.doi.org/10.1016/j.progpolymsci.2010.11.003.
[53] S. Mohanty, S.K. Nayak, Effect of clay exfoliation and organic modification on morphological, dynamic mechanical, and thermal behavior of melt-compounded polyamide-6 nanocomposites, Polym. Compos. 28 (2007) 153–162, http://dx.doi.org/10.1002/pc.20284.
[54] M.R. Ayatollahi, S. Shadlou, M.M. Shokrieh, M. Chitsazzadeh, Effect of multi-walled carbon nanotube aspect ratio on mechanical and electrical properties of epoxy-based nanocomposites, Polym. Test. 30 (2011) 548–556, http://dx.doi.org/10.1016/j.polymertesting.2011.04.008.
[55] C.-W. Nan, Y. Shen, J. Ma, Physical properties of composites near percolation, Annu. Rev. Mater. Res. 40 (2010) 131–151, http://dx.doi.org/10.1146/annurev-matsci-070909-104529.
[56] H. Palza, C. Garzón, O. Arias, Modifying the electrical behaviour of polypropylene/carbon nanotube composites by adding a second nanoparticle and by annealing processes, Express Polym. Lett. 6 (2012) 639–646, http://dx.doi.org/10.3144/expresspolymlett.2012.68.

[57] Y. Pan, L. Li, Percolation and gel-like behavior of multiwalled carbon nanotube/polypropylene composites influenced by nanotube aspect ratio, Polymer (Guildf) 54 (2013) 1218–1226, http://dx.doi.org/10.1016/j.polymer.2012.12.058.
[58] Y. Li, J. Zhu, S. Wei, J. Ryu, Q. Wang, L. Sun, et al, Poly(propylene) nanocomposites containing various carbon nanostructures, Macromol. Chem. Phys. 212 (2011) 2429–2438, http://dx.doi.org/10.1002/macp.201100364.
[59] S.C. Tjong, G.D. Liang, S.P. Bao, Electrical behavior of polypropylene/multiwalled carbon nanotube nanocomposites with low percolation threshold, Scr. Mater. 57 (2007) 461–464, http://dx.doi.org/10.1016/j.scriptamat.2007.05.035.
[60] M. Wen, X. Sun, L. Su, J. Shen, J. Li, S. Guo, The electrical conductivity of carbon nanotube/carbon black/polypropylene composites prepared through multistage stretching extrusion, Polymer (Guildf) 53 (2012) 1602–1610, http://dx.doi.org/10.1016/j.polymer.2012.02.003.
[61] M.A. Garza-Navarro, M. Hinojosa-Rivera, V. González-González, Desarrollo de nanocompuestos superparamagnéticos quitosán/magnetita, Ingenierías 9 (2006) 14–20.
[62] J. Alam, U. Riaz, S. Ahmad, Effect of ferrofluid concentration on electrical and magnetic properties of the Fe_3O_4/PANI nanocomposites, J. Magn. Magn. Mater. 314 (2007) 93–99, http://dx.doi.org/10.1016/j.jmmm.2007.02.195.